Supplementary material

S1. Synthetic validation and computational performance

Tables S1 and S2 and Fig. S1 document the processing configuration and synthetic validation experiments E1–E5. Computational performance is reported separately in Table S3.

Table S1. Processing parameters used in the synthetic validation (E1–E5). The configuration was selected on an independent tuning set (Section 2.2, Fig. S1) and used without modification in all experiments. The upper block lists the parameters exposed in the graphical interface; the lower block lists settings fixed in the implementation. Values for the experimental recordings of Sections 3.2 and 3.3 are given in the last column; the spatial calibration was set separately for each dataset (4.49, 5.32, and 13.957 µm px^{-1} for Sects. 3.2, 3.3 Injector 1, and 3.3 Injector 2, respectively).

Stage	Parameter	OpenCV function / argument	Value (E1–E5)	Value (experimental, Sects. 3.2–3.3)	User-configurable
Preprocessing	Contrast enhancement method	-	CLAHE	Percentile stretching	Yes
Preprocessing	CLAHE clip limit	cv2.createCLAHE clipLimit	2	– (not used)	Yes
Preprocessing	Non-Local Means filter strength h	cv2.fastNlMeansDenoising h	30	8	Yes
Segmentation	Adaptive threshold block size (px)	cv2.adaptiveThreshold blockSize	11	19	Yes
Segmentation	Adaptive threshold constant C	cv2.adaptiveThreshold C	5	4	Yes
Segmentation	Elliptical structuring element size (px)	cv2.getStructuringElement ksize	3	2	Yes
Filtering	Minimum projected area (px^2)	-	15	15	Yes
Filtering	Maximum projected area (px^2)	-	8000	5000	Yes
Filtering	Minimum circularity	-	0.5	0.25	Yes
Filtering	Minimum roundness	-	0	0	Yes

Stage	Parameter	OpenCV function / argument	Value (E1–E5)	Value (experimental, Sects. 3.2–3.3)	User-configurable
Tracking	Maximum association distance (px)	-	15	6	Yes
Tracking	Lucas–Kanade position prediction	-	Yes	Yes	Yes
Tracking	Lucas–Kanade window size (px)	cv2.calcOpticalFlowPyrLK winSize	15	15	Yes
Preprocessing	Grayscale conversion	cv2.cvtColor (COLOR_BGR2GRAY)	-	Same	No
Preprocessing	CLAHE tile grid size	cv2.createCLAHE tileGridSize	8 × 8	– (not used)	No
Preprocessing	Percentile stretching limits	np.percentile	0.4 % / 99.6 %	Same	No
Preprocessing	NL-Means template / search window	cv2.fastNlMeansDenoising	7 px / 21 px (OpenCV defaults)	Same	No
Segmentation	Adaptive method / polarity	cv2.adaptiveThreshold	ADAPTIVE_THRESH_GAUSSIAN_C, THRESH_BINARY_INV	Same	No
Segmentation	Structuring element shape	cv2.getStructuringElement	MORPH_ELLIPSE	Same	No
Segmentation	Morphological sequence	cv2.morphologyEx	opening, then closing (same kernel)	Same	No
Contours	Pass 1 (hole filling)	cv2.findContours	RETR_EXTERNAL, CHAIN_APPROX_SIMPLE; contours with A > min area filled	Same	No
Contours	Pass 2 (measurement)	cv2.findContours	RETR_EXTERNAL, CHAIN_APPROX_NONE	Same	No
Features	Circularity	$4\pi A/P^2$ (cv2.contourArea, cv2.arcLength)	clipped to ≤ 1	Same	No
Features	Roundness	$4A/(\pi \cdot MA^2)$ (cv2.fitEllipse)	requires ≥ 5 contour points; clipped to ≤ 1	Same	No
Features	Centroid	cv2.moments	bounding-box centre if M00 = 0	Same	No
Tracking	Lucas–Kanade pyramid levels	cv2.calcOpticalFlowPyrLK maxLevel	2	Same	No
Tracking	Lucas–Kanade stop criteria	cv2.calcOpticalFlowPyrLK criteria	10 iterations or $\varepsilon = 0.03$	Same	No

Stage	Parameter	OpenCV function / argument	Value (E1–E5)	Value (experimental, Sects. 3.2–3.3)	User-configurable
Tracking	Maximum gap before a track is closed	-	5 frames	Same	No
Tracking	Association	-	greedy nearest neighbour, one detection per track and frame	Same	No

Table S2. Configuration of the synthetic sequences. All frames are 512 × 512 px, with dark droplets (core grey level 25) on a bright background (grey level 235), a Gaussian edge profile with σedge = 0.8 px, lossless FFV1 encoding, and a noise seed derived from the sequence name. Velocities in px/frame. The tuning set is disjoint from E1–E5 in diameters, noise realizations, and droplet layouts.

Set	Content	d_{GT} (px)	Velocity (px/frame)	Noise	Frames
E1	Static droplets, 4 per frame (2 × 2 grid)	6, 10, 15, 20, 30, 40, 50	0	None	30
E2	Single moving droplet	20	(2, 0), (5, 0), (0, 3), (3, 3), (−4, 2), (1.3, 0.7), (4.25, −1.6), (0.4, 0), (0.2, 0)	None; Gaussian σ = 8	60
E3	Single static droplet	20	0	Gaussian σ = 0, 5, 10, 20, 35, 50; salt-and-pepper 0, 2, 5, 10%	40
E4	Single static droplet	3, 4, 5, 6, 8, 10, 12, 15, 20, 25, 30, 40, 50, 60, 70, 80	0	Gaussian σ = 8	30
E5	5, 10, 20, 35, 50 droplets, random positions and directions (layout seed 72)	18	|v| = 3, random direction	Gaussian σ = 8	60
Tuning	Static 2 × 2 grid; 10 and 25 moving droplets (layout seed 2024); isolated droplet	5, 9, 14, 25, 45 (static); 16 (moving)	0; |v| = 3; (4.5, 4.0)	Gaussian σ = 0, 10, 25; salt-and-pepper 5%; σ = 8 (moving)	10 (static); 40 (moving)

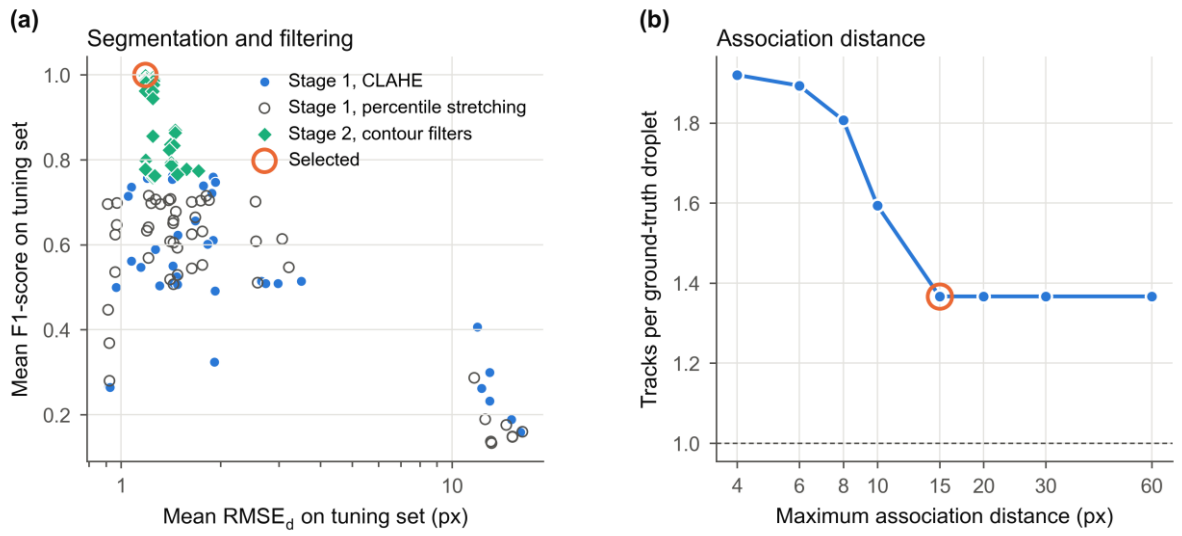

Figure S1. Selection of the processing configuration on the independent tuning set. (a) Mean F1-score versus mean diameter RMSE for the 96 segmentation configurations of stage 1 (CLAHE, filled; percentile stretching, open) and the 36 combinations of minimum area and circularity of stage 2 (diamonds); the selected configuration is circled. Configurations with low F1-scores in stage 1 lose small droplets or produce noise-induced false positives at σ = 25, which the contour filters of stage 2 remove. (b) Mean number of reconstructed tracks per ground-truth droplet on the moving-droplet tuning sequences as a function of the maximum association distance; the selected value (15 px) is the smallest one at which fragmentation stops decreasing.

Table S3. Processing time of Droplet Analyzer per pipeline stage (median of three runs). Intel Core i7-9700F CPU (3.0 GHz), OpenCV 4.12, configuration of Table S1. Percentages refer to the total processing time; writing of output files is excluded. Preprocessing comprises grayscale conversion, CLAHE, and Non-Local Means denoising.

Recording	Size (px)	Frames	Frames/s	ms/frame	Decoding (%)	Pre-processing (%)	Threshold + morphology (%)	Contours + features (%)	Tracking (%)
Experimental, Camera1_18_58_03	312 × 260	102	9.08	110.1	0.37	98.69	0.28	0.41	0.24
Experimental, Camera1_19_12_56	312 × 260	102	9.17	109.1	0.35	99.29	0.28	0.05	0.02
Experimental, Camera1_19_18_43	312 × 260	102	9.14	109.4	0.35	99.31	0.28	0.04	0.01
Synthetic E5, $N_d = 50$	512 × 512	60	5.74	174.1	0.46	95.83	0.56	1.89	1.24
Synthetic E1, $d_{GT} = 20$ px	512 × 512	30	5.92	168.9	0.31	98.54	0.57	0.25	0.33

S2. Experimental trajectory screening

The experimental droplet trajectories reconstructed by Droplet Analyzer were subjected to a screening procedure before calculating the droplet size and velocity statistics. Single-frame trajectories were excluded because they did not provide sufficient information for displacement-based velocity estimation. Trajectories exhibiting nearly stationary motion, physically implausible velocities or displacement jumps, or motion opposite to the main spray direction were also screened. A minimum trajectory speed of 1 m/s was adopted as a practical criterion for removing nearly stationary detections. The archived cleaning procedure also included a morphological criterion for trajectories lasting no more than four frames, rejecting those that originated in the image interior and exhibited mean circularity below 0.25 or mean roundness below 0.20. Extreme droplet diameters were flagged for review but were not automatically excluded on the basis of size alone.

The experiments were recorded at 10^6 frames/s. Droplet positions and velocities were expressed using the spatial calibrations of 5.32 μm/pixel for Injector 1 and 13.957 μm/pixel for Injector 2. At this acquisition frequency, the minimum-speed threshold of 1 m/s corresponds to interframe displacements of approximately 0.188 and 0.0716 pixels, respectively (Table S4). The threshold was used for practical data screening and was not derived from the accuracy limits established in the isolated-droplet validation experiment E2.

Following trajectory screening, the data were restricted to the normalized transverse region $0 \leq \xi \leq 0.5$, where $\xi = |r|/D$, $|r|$ is the absolute mean transverse distance from the spray axis, and D is the nominal discharge orifice diameter. The final datasets comprised 1254 trajectories for Injector 1 and 1954 for Injector 2. The resulting 3208 trajectories were grouped by injector, applied voltage, and five transverse regions, producing 70 local populations for the droplet size analysis. Each trajectory contributed one representative equivalent diameter to the calculation of the local statistics, independently of its duration in frames. Table S1 reports a minimum contour-area setting of 15 px^2, corresponding to an equivalent diameter of 4.37 px. The smallest representative diameter in the retained experimental population is 6.18 px, equivalent to a circular area of 30 px^2 and to 32.9 and 86.3 μm for Injectors 1 and 2, respectively (Table S4). This lower boundary is already present in the processed trajectory datasets before the final selection within $0 \leq \xi \leq 0.5$. Its origin in the processing chain has not been established, and it should not be interpreted as a validated detection limit. The reported size statistics do not characterize droplets below this boundary.

Table S4. Experimental trajectory screening and data selection for the two Flow Blurring injectors. The reported counts correspond to successive processing stages. The final analysis was restricted to the normalized transverse interval $0 \leq \xi \leq 0.5$. The differences between the reported spatial subsets and the final retained populations are shown separately because the corresponding individual exclusion records are unavailable. The last two rows give the smallest equivalent diameter among the retained trajectories.

Parameter	Injector 1	Injector 2
Acquisition frequency (frames/s)	10^6	10^6
Spatial calibration (μm/pixel)	5.32	13.957
Minimum-speed screening criterion (m/s)	1.0	1.0
Equivalent displacement at 1 m/s (pixel/frame)	0.188	0.0716
Initially reconstructed trajectories	8991	17405
Trajectories after initial screening	3598	11219
Trajectories after additional filtering	3516	11138
Trajectories within $0 \leq \xi \leq 0.5$	1308	2043
Trajectories not carried forward after spatial selection	54	89
Final retained trajectories	**1254**	**1954**
Retention relative to cleaned dataset (%)	35.7	17.5
Retention relative to initial dataset (%)	13.9	11.2
Minimum retained equivalent diameter (pixel)	6.18	6.18
Minimum retained equivalent diameter (μm)	32.9	86.3

S3. Pneumatic Flow Blurring reference calculations

This section documents the fixed pneumatic reference diameters compared with the local experimental measurements in Fig. 7 of the main text. Injector 1 corresponds to the 700 μm orifice and Injector 2 to the 900 μm orifice. LCP gas conditions were estimated using the ideal gas isentropic approximation described in Sect. 2.3.4.

S3.1. Geometry and gas mass flow

For the nominal lateral cylindrical passage,

$$A_{\mathrm{LCP}} = \pi D H, \qquad \dot{m}_g = \rho_g Q_g, \qquad G = \frac{\dot{m}_g}{A_{\mathrm{LCP}}}.$$

Using $D = 700$ and 900 μm, and $H = 50$ μm for the two injectors, the areas are 1.0996×10^{-7} and 1.4137×10^{-7} m^2. The input gas flow rates are 0.8047 and 2.33 L min^{-1} and are converted to gas mass flow using $\rho_{g,ref} = 1.20$ kg m^{-3}. This gives $\dot{m}_g = 1.6094 \times 10^{-5}$ and 4.6600×10^{-5} kg s^{-1}, respectively, and $G = 146.37$ and 329.63 kg m^{-2} s^{-1}.

S3.2. Estimated gas conditions at the LCP

For ideal-gas, isentropic expansion at $T_0 = 296.15$ K, $P_a = 101325$ Pa, $R = 287.05$ J kg^{-1} K^{-1}, and $\gamma_c = 1.4$,

$$T_g = \frac{T_0}{1 + aM^2}, \quad \rho_g = \frac{P_a}{RT_g}, \quad U_g = M\sqrt{\gamma_c R T_g}, \quad a = \frac{\gamma_c - 1}{2}.$$

Mass conservation gives

$$C = \frac{G\sqrt{RT_0}}{P_a\sqrt{\gamma_c}}, \qquad C^2 = M^2(1 + aM^2), \qquad M^2 = \frac{-1 + \sqrt{1 + 4aC^2}}{2a}.$$

Finally,

$$P_0 = P_a(1 + aM^2)^{\gamma_c/(\gamma_c - 1)}, \qquad \Delta P = P_0 - P_a.$$

The model-inferred gas velocities are 119.8 and 248.0 m s^{-1}, with corresponding inferred ΔP values of 9.04 and 47.10 kPa. These values rely on the nominal passage geometry and on treating the LCP static pressure as ambient; they are not measurements of the internal gas field or pressure drop.

S3.3. Reference droplet diameters

Using $\rho_l = 997$ kg m^{-3}, $\mu_l = 8.9 \times 10^{-4}$ Pa s, and $\sigma = 0.072$ N m^{-1},

$$GLR = \frac{\rho_{g,ref} Q_g}{\rho_l Q_l}, \qquad We_D = \frac{\rho_g U_g^2 D}{2\sigma}, \qquad Oh_D = \frac{\mu_l}{\sqrt{\rho_l \sigma D}},$$

and

$$D_{\mathrm{FB}} = 0.42D\,We_D^{-0.6}(1 + 18Oh_D)(1 + GLR^{-1})^{1.2}.$$

The Rosell-Llompart and Gañán-Calvo scale is

$$d_0 = \frac{\sigma}{\Delta P}, \quad Q_0 = \left(\frac{\sigma^4}{\rho_l \Delta P^3}\right)^{1/2}, \quad d_{\mathrm{FB,min}} = 1.42 d_0 \left(\frac{Q_l}{Q_0}\right)^{1/5}.$$

Table S5. Input quantities and calculated pneumatic Flow Blurring reference scales.

Quantity	Injector 1	Injector 2
D (µm)	700	900
H (µm)	50	50
H/D	0.0714	0.0556
Q_l (mL min^{-1})	4.062	19.722
Q_g (L min^{-1})	0.8047	2.33
A_{LCP} (m^2)	1.0996×10^{-7}	1.4137×10^{-7}
$\dot{m}_g$ (kg s^{-1})	1.6094×10^{-5}	4.6600×10^{-5}
G (kg m^{-2} s^{-1})	146.37	329.63
M	0.352	0.759
T_g (K)	289.0	265.5
ρ_g (kg m^{-3})	1.221	1.329
U_g (m s^{-1})	119.8	248.0
ΔP (kPa), inferred	9.04	47.10
GLR	0.2384	0.1422
We_D	85.27	510.87
Oh_D	0.00397	0.00350
D_{FB} (µm)	157.9	116.1
d_0 (µm)	7.961	1.529
Q_0 (mL min^{-1})	0.01145	0.000964
$d_{\mathrm{FB,min}}$ (µm)	36.6	15.8

The LCP velocity, density, and inferred pressure difference depend on the stated ideal-gas approximation and nominal geometry. The corresponding diameters are reference scales, not direct local measurements.

S4. Local droplet-size statistics

S4.1. Injector conditions

Two electrically assisted Flow Blurring injectors were analyzed over seven applied voltages (0, 2, 4, 6, 8, 10, and 12 kV). The analysis uses one representative diameter and one representative transverse position per accepted reconstructed trajectory.

Table S6. Geometry and spatial calibration of the two Flow Blurring injectors.

Injector	D (μm)	H (μm)	H/D	Spatial calibration (μm/px)
1	700	50	0.0714	5.32
2	900	50	0.0556	13.957

The number of recordings represented in the final processed master dataset is not identical for every voltage. Injector 1 contains four recordings at 0, 2, 4, 6, 8, and 12 kV and three at 10 kV. Injector 2 contains three recordings at 0, 2, 4, 8, 10, and 12 kV and five at 6 kV.

S4.2. Transverse coordinate and grouping

For every accepted track, the absolute transverse distance from the spray axis is converted to the dimensionless coordinate

$$\xi = |r| / D$$

where $|r|$ is the track-level mean transverse distance from the spray axis and D is the nominal discharge-orifice diameter. Five common intervals are used for both injectors:

$$[0, 0.1), [0.1, 0.2), [0.2, 0.3), [0.3, 0.4), [0.4, 0.5]$$

A track exactly at $\xi = 0.5$ is retained in the fifth bin. The previously existing η and radial zone columns in the source master files are not used because they were based on a different normalization.

S4.3. Local size statistics

For each injector, voltage, and transverse interval, the mean position is calculated from the accepted trajectories. Each trajectory contributes once to the diameter statistics. The same calculations are repeated for individual recordings to characterize experimental repeatability.

Sauter mean diameter: $D32 = \Sigma Di^3 / \Sigma Di^2$.

Volume median diameter: diameters are sorted in ascending order and weighted by Di^3. Dv50 is the first diameter for which the cumulative D^3 weight reaches 0.5.

The same calculations are repeated independently for each recording and radial bin to quantify run-to-run variability. These replicate-level statistics are descriptive measures of repeatability; they are not treated as standard errors of the local statistics.

The resulting dataset contains 3208 trajectories and 70 local groups. Independent-recording statistics cover 250 recording–interval groups; 40 contain five or fewer trajectories.

Table S7. Local droplet-size statistics across independent recordings

For each injector, voltage, and transverse interval, the table reports the unweighted mean and sample standard deviation of D32 and Dv50 across independent recordings. n denotes the number of recordings and N the total number of accepted trajectories. These statistics describe between-recording variability; the characteristic diameters in Fig. 7 are calculated from all accepted trajectories within each group.

Injector	Voltage (kV)	ξ interval	n	N tracks	mean ξ	D32 (μm), mean ± SD	Dv50 (μm), mean ± SD
1	0	0–0.1	4	31	0.055	117.0 ± 55.5	145.4 ± 79.8
1	0	0.1–0.2	4	35	0.154	97.0 ± 53.8	105.7 ± 58.3
1	0	0.2–0.3	4	67	0.249	75.8 ± 16.7	93.4 ± 28.3
1	0	0.3–0.4	4	26	0.350	100.2 ± 29.1	125.8 ± 41.1
1	0	0.4–0.5	4	45	0.449	53.8 ± 11.2	60.2 ± 21.4
1	2	0–0.1	4	38	0.049	56.7 ± 9.5	61.2 ± 12.0
1	2	0.1–0.2	4	45	0.160	77.2 ± 28.6	99.0 ± 48.6
1	2	0.2–0.3	4	38	0.239	69.5 ± 18.2	89.6 ± 30.2
1	2	0.3–0.4	4	22	0.349	60.4 ± 7.9	73.6 ± 13.6
1	2	0.4–0.5	4	28	0.450	95.8 ± 67.4	116.0 ± 82.1
1	4	0–0.1	4	47	0.040	77.2 ± 19.0	81.3 ± 20.1
1	4	0.1–0.2	4	45	0.148	56.0 ± 7.2	59.1 ± 10.9
1	4	0.2–0.3	4	51	0.243	83.0 ± 26.9	104.1 ± 25.1
1	4	0.3–0.4	4	34	0.344	86.4 ± 54.9	93.2 ± 55.3
1	4	0.4–0.5	4	42	0.444	83.2 ± 32.9	98.6 ± 52.5
1	6	0–0.1	4	41	0.041	90.4 ± 33.8	112.0 ± 50.4
1	6	0.1–0.2	4	37	0.146	60.4 ± 5.0	61.9 ± 2.8
1	6	0.2–0.3	4	52	0.242	73.1 ± 31.9	78.0 ± 37.6
1	6	0.3–0.4	4	33	0.348	80.5 ± 34.7	100.3 ± 51.6
1	6	0.4–0.5	4	25	0.446	63.3 ± 20.0	69.3 ± 26.7
1	8	0–0.1	4	41	0.060	64.2 ± 11.8	69.2 ± 13.9
1	8	0.1–0.2	4	25	0.143	90.4 ± 43.9	101.8 ± 50.5
1	8	0.2–0.3	4	29	0.247	99.7 ± 15.9	128.8 ± 12.1
1	8	0.3–0.4	4	24	0.362	79.2 ± 16.7	103.1 ± 31.4
1	8	0.4–0.5	4	38	0.453	92.1 ± 25.2	119.9 ± 43.4
1	10	0–0.1	3	15	0.039	53.9 ± 16.0	57.1 ± 19.0
1	10	0.1–0.2	3	13	0.165	59.3 ± 14.5	64.5 ± 19.2
1	10	0.2–0.3	3	48	0.258	71.9 ± 10.7	76.6 ± 11.4
1	10	0.3–0.4	3	28	0.344	69.4 ± 21.8	78.6 ± 30.9
1	10	0.4–0.5	3	24	0.459	65.3 ± 9.8	78.2 ± 22.9
1	12	0–0.1	4	23	0.045	54.1 ± 9.6	62.9 ± 19.4
1	12	0.1–0.2	4	45	0.157	50.3 ± 4.8	50.1 ± 5.1

Injector	Voltage (kV)	ξ interval	n	N tracks	mean ξ	D32 (µm), mean ± SD	Dv50 (µm), mean ± SD
1	12	0.2–0.3	4	32	0.241	52.7 ± 7.1	59.6 ± 11.0
1	12	0.3–0.4	4	51	0.347	48.7 ± 4.9	49.0 ± 3.1
1	12	0.4–0.5	4	36	0.445	48.1 ± 2.9	55.1 ± 7.6
2	0	0–0.1	3	52	0.053	156.1 ± 23.5	211.3 ± 29.6
2	0	0.1–0.2	3	64	0.155	157.5 ± 21.7	182.6 ± 25.2
2	0	0.2–0.3	3	76	0.244	139.6 ± 28.5	146.4 ± 50.1
2	0	0.3–0.4	3	47	0.342	156.6 ± 23.2	194.3 ± 67.1
2	0	0.4–0.5	3	58	0.443	155.2 ± 29.4	168.3 ± 62.4
2	2	0–0.1	3	48	0.053	199.3 ± 54.1	221.8 ± 52.2
2	2	0.1–0.2	3	59	0.147	156.4 ± 19.1	192.1 ± 45.4
2	2	0.2–0.3	3	63	0.251	145.3 ± 21.6	160.3 ± 42.2
2	2	0.3–0.4	3	52	0.351	120.4 ± 10.2	119.8 ± 15.3
2	2	0.4–0.5	3	43	0.453	138.3 ± 7.6	146.5 ± 9.1
2	4	0–0.1	3	75	0.053	176.4 ± 23.2	213.3 ± 62.1
2	4	0.1–0.2	3	68	0.143	160.2 ± 47.5	178.0 ± 66.0
2	4	0.2–0.3	3	40	0.248	143.2 ± 18.6	157.9 ± 20.2
2	4	0.3–0.4	3	65	0.348	164.3 ± 45.9	203.3 ± 85.1
2	4	0.4–0.5	3	45	0.450	115.1 ± 6.3	119.4 ± 22.4
2	6	0–0.1	5	68	0.055	128.8 ± 17.4	139.6 ± 29.5
2	6	0.1–0.2	5	76	0.153	130.9 ± 20.4	128.0 ± 18.9
2	6	0.2–0.3	5	72	0.248	165.6 ± 27.1	198.3 ± 58.9
2	6	0.3–0.4	5	91	0.349	136.3 ± 33.1	144.2 ± 56.2
2	6	0.4–0.5	5	62	0.452	121.1 ± 19.9	123.5 ± 24.4
2	8	0–0.1	3	50	0.058	131.8 ± 11.8	139.6 ± 20.6
2	8	0.1–0.2	3	36	0.151	126.9 ± 21.3	132.3 ± 26.5
2	8	0.2–0.3	3	60	0.251	129.3 ± 22.2	126.9 ± 20.3
2	8	0.3–0.4	3	51	0.348	163.1 ± 35.0	214.3 ± 116.4
2	8	0.4–0.5	3	59	0.447	126.8 ± 4.0	126.4 ± 5.7
2	10	0–0.1	3	62	0.058	113.7 ± 9.8	113.7 ± 17.5
2	10	0.1–0.2	3	53	0.141	135.8 ± 23.9	168.9 ± 73.3
2	10	0.2–0.3	3	51	0.256	140.2 ± 29.6	151.7 ± 47.9
2	10	0.3–0.4	3	69	0.345	133.0 ± 22.5	145.0 ± 29.0
2	10	0.4–0.5	3	44	0.451	122.9 ± 12.7	124.7 ± 14.8
2	12	0–0.1	3	42	0.053	124.0 ± 30.2	151.2 ± 81.3
2	12	0.1–0.2	3	40	0.150	117.9 ± 13.2	111.8 ± 12.2
2	12	0.2–0.3	3	34	0.256	125.0 ± 12.5	147.9 ± 45.2
2	12	0.3–0.4	3	32	0.356	104.6 ± 14.4	100.7 ± 13.3
2	12	0.4–0.5	3	47	0.449	121.1 ± 22.7	114.2 ± 14.1

Note: 40 of the 250 recording–region groups contain five or fewer trajectories. The standard deviations describe repeatability across recordings rather than errors in the diameter statistics.

S5. Additional analysis of the voltage response

This section complements Sects. 3.3.4 and 3.3.5 of the main text. It uses the same 3208 trajectories and the same 70 local populations. Diameter quantiles follow the definitions of Sect. S4.3.

Sampling intervals were obtained with a two-stage resampling that respects the recording structure. For each injector and voltage, the recordings were drawn with replacement, and the trajectories of each drawn recording were then drawn with replacement within each transverse region. The same recordings were used for all regions and for the all-region population of that voltage (all trajectories of the injector at that voltage, from the five regions within $0 \leq \xi \leq 0.5$). Ratios with respect to 0 kV were obtained by combining independent resamples of the energized and zero-voltage conditions. The procedure was repeated 3000 times, and 95% percentile intervals are reported. Each condition contains 3 to 5 recordings (Sect. S4.1) and each local population 13 to 91 trajectories, so the intervals are approximate and are given as an indication of sampling variability. They do not include variability of the experimental conditions beyond that contained in the recordings, and they are not used to establish statistical significance. Because the local intervals are wide, the figures of this section are descriptive.

S5.1. Relative span of the local size distribution

The relative span of the volume-based distribution is

$$\mathrm{RSF}_v(V, Z_j) = \frac{D_{v90}(V, Z_j) - D_{v10}(V, Z_j)}{D_{v50}(V, Z_j)}.$$

Figure S2 shows RSF_v for each transverse region. Local values lie between 0.48 and 1.30 for Injector 1 and between 0.60 and 1.42 for Injector 2. At 12 kV, RSF_v ranges from 0.48 to 0.91 for Injector 1 (0 kV, 0.63 to 0.91) and from 0.77 to 1.25 for Injector 2 (0 kV, 0.72 to 1.06). The local estimates have substantial sampling uncertainty, and the intervals at 0 and 12 kV overlap in all ten regions (Table S8). The local values show no common monotonic progression with voltage. The overlap of the separate sampling intervals at 0 and 12 kV describes the variability of the local estimates but does not directly quantify the uncertainty in their difference. For all regions combined, RSF_v changes from 1.22 to 0.70 for Injector 1 and from 0.86 to 1.30 for Injector 2 between 0 and 12 kV; the 95% sampling intervals of these changes (−1.23 to 0.08 and −0.57 to 0.61) include zero, so the data do not establish a change in relative width. The lower quantile D_{v10} lies close to the minimum diameter (Sect. S2). Truncation at this limit can affect all quantiles and RSF_v, and the direction of this effect is not established by the present data.

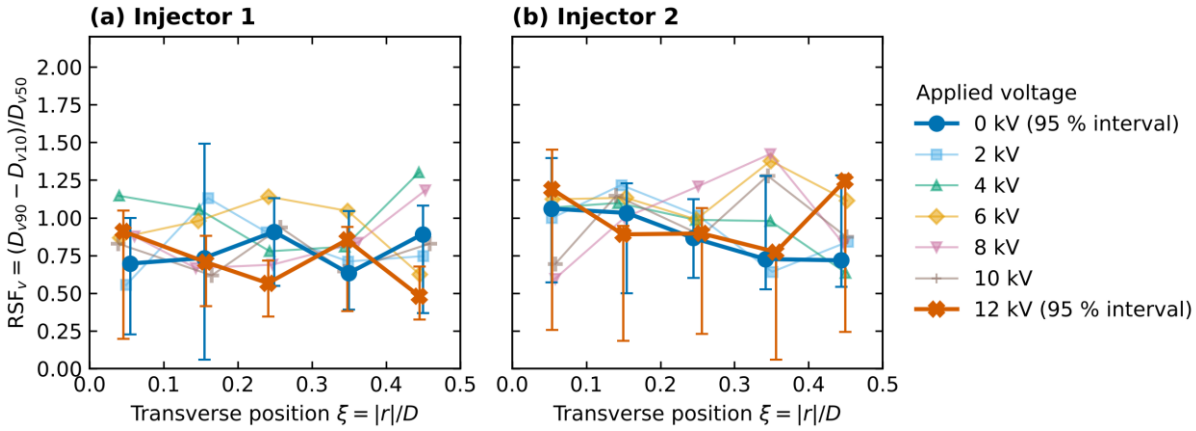

Figure S2. Relative span of the volume-based droplet size distribution, $RSF_v = (D_{v90} - D_{v10})/D_{v50}$, as a function of the normalized transverse position $\xi = |r|/D$ for (a) Injector 1 and (b) Injector 2. Error bars show 95% sampling intervals obtained by resampling recordings and then trajectories (Sect. S5) and are drawn for 0 and 12 kV only. Lines connect symbols to guide the eye. D_{v10} lies close to the minimum retained diameter of 6.18 px (Sect. S2).

S5.2. Response against the measured net current

The net electrical current I_{net} was measured with an aluminium electrode of honeycomb geometry placed approximately 15 cm downstream of the injector. The honeycomb structure allowed the liquid to pass through the electrode, which was reached by the whole spray, so that the current was measured at that location for each applied voltage. Current measurements were obtained during the same experimental sessions as the ultra-high-speed recordings. For each injector, the net current was calculated by subtracting the mean signed current measured at 0 kV from the mean signed current at each applied voltage. The zero-voltage references were −0.210 nA for Injector 1 and 8.10 nA for Injector 2. The absolute value of the resulting net current was used to calculate I^*. This correction removes the zero-voltage baseline but does not separate the contributions of droplets, ions, or voltage-dependent leakage to the measured current.

The measured net current was normalized as

$$I^* = \frac{|I_{\mathrm{net}}|}{\sqrt{\sigma_l \kappa_l Q_l}},$$

where κ_l is the electrical conductivity of the liquid (2.2 µS cm^{-1} = 2.2 × 10^{-4} S m^{-1}, Table 1 of the main text) and Q_l is the liquid flow rate (4.062 and 19.722 mL min^{-1} for Injectors 1 and 2, Table S5). The denominator is the electrical current scale commonly used for charged liquid jets (Gañán-Calvo et al., 1997; Gañán-Calvo, 2004). At 12 kV, I_{net} was 8.51 µA for Injector 1 and 21.3 µA for Injector 2, which correspond to I^* of 8.2 and 9.3. Because the two values of I^* are similar at 12 kV, the two injectors can be compared at nearly the same value of this coordinate, which does not establish equivalent charge states or atomization conditions. The net current is a global measurement made approximately 15 cm downstream of the injector, whereas the droplet sizes were obtained within the observed region around 3 cm downstream (Table 1 of the main text), and it does not identify the contribution of the droplets alone.

The local response of the Sauter mean diameter is expressed as

$$\mathcal{R}_{32}(V, Z_j) = \frac{D_{32}(V, Z_j)}{D_{32}(0, Z_j)}.$$

Figure S3 shows $\mathcal{R}_{32}$ against I^* for each transverse region. At 12 kV, all ten point estimates of $\mathcal{R}_{32}$ are below unity (Table S8). For Injector 1 they lie between 0.36 and 0.80, and the sampling interval includes unity only in Z5. For Injector 2 they lie between 0.74 and 0.88, and the intervals include unity in Z1, Z3, and Z5. In Z5, Injector 1 shows $\mathcal{R}_{32}$ above unity at all voltages from 2 to 10 kV, a behavior not seen in Injector 2. At the same I^* of about 8 to 9, the two injectors differ in $\mathcal{R}_{32}$, and the current normalized in this way does not place them on one curve either.

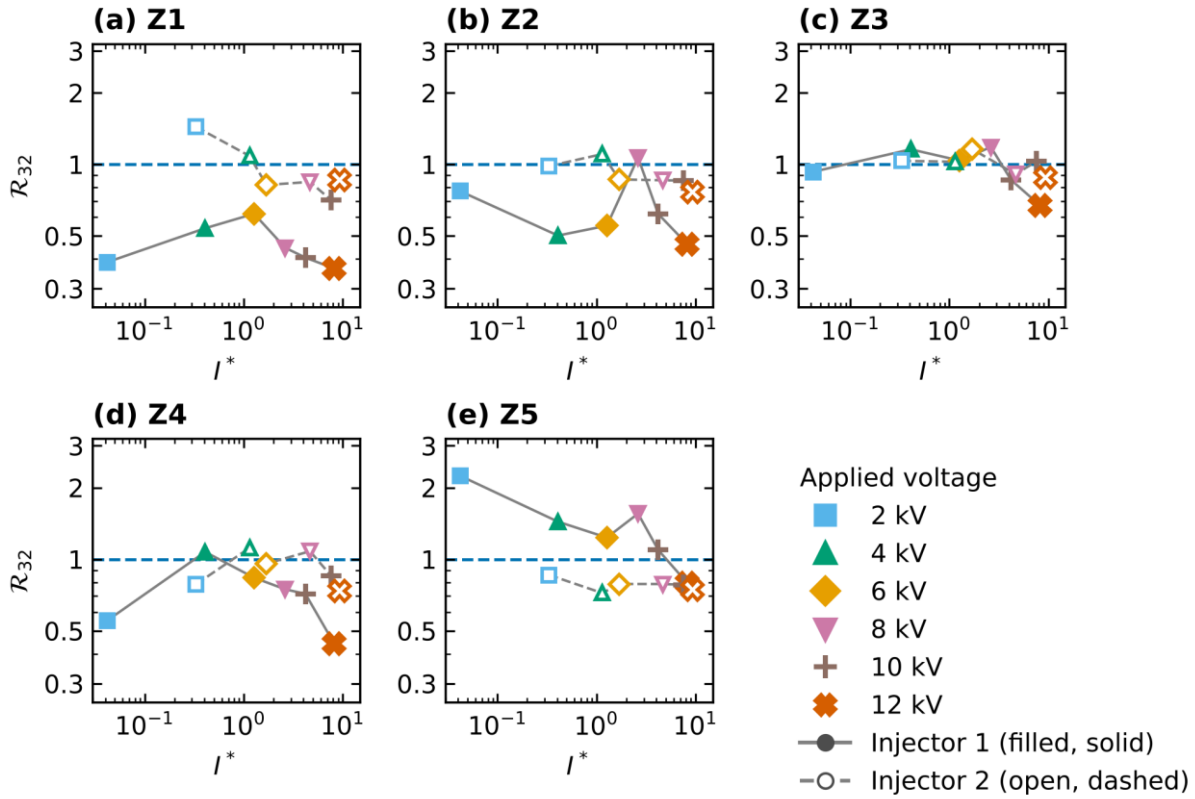

Figure S3. Ratio of the local Sauter mean diameter to its value at 0 kV, $\mathcal{R}_{32}$, as a function of the normalized net current I^* for transverse regions (a) Z1, (b) Z2, (c) Z3, (d) Z4, and (e) Z5. Filled symbols and solid lines correspond to Injector 1 and open symbols and dashed lines to Injector 2. Symbols and colors indicate the applied voltage. The dashed horizontal line indicates $\mathcal{R}_{32}$ = 1. The vertical axis is logarithmic. Intervals for 12 kV are given in Table S8.

Table S8. Local response of the Sauter mean diameter at 12 kV, $\mathcal{R}_{32}$, and relative span of the volume distribution, RSF_v, at 0 and 12 kV for each injector and transverse region. Values in brackets are 95% percentile sampling intervals obtained by resampling recordings and then trajectories (Sect. S5).

Injector	Region	$\mathcal{R}_{32}$ (12 kV)	RSF_v (0 kV)	RSF_v (12 kV)
1	Z1	0.36 [0.27, 0.79]	0.70 [0.23, 1.00]	0.91 [0.20, 1.05]
1	Z2	0.46 [0.30, 0.83]	0.73 [0.06, 1.49]	0.71 [0.41, 0.88]
1	Z3	0.67 [0.54, 0.91]	0.91 [0.55, 1.13]	0.57 [0.35, 0.72]
1	Z4	0.44 [0.36, 0.71]	0.63 [0.39, 1.04]	0.85 [0.38, 0.94]
1	Z5	0.80 [0.68, 1.11]	0.89 [0.37, 1.08]	0.48 [0.32, 0.68]
2	Z1	0.86 [0.57, 1.24]	1.06 [0.57, 1.39]	1.19 [0.25, 1.45]
2	Z2	0.76 [0.60, 0.96]	1.03 [0.50, 1.23]	0.89 [0.18, 0.95]
2	Z3	0.88 [0.68, 1.17]	0.87 [0.60, 1.12]	0.90 [0.23, 1.06]
2	Z4	0.74 [0.54, 0.96]	0.73 [0.52, 1.28]	0.77 [0.06, 0.79]
2	Z5	0.74 [0.57, 1.09]	0.72 [0.54, 1.28]	1.25 [0.24, 1.29]

S5.3. All-region response and apparent specific charge

The all-region values of this section are calculated from all accepted trajectories of each injector at a given voltage, combining the five transverse regions ($0 \leq \xi \leq 0.5$). They do not represent a distribution integrated over the whole spray or weighted by liquid flow, and combining the regions does not remove their heterogeneity or increase the number of independent recordings. Figure S4a shows the all-region Sauter diameter normalized by the orifice diameter, D_{32}/D, against I^*. At 0 kV the values are 0.152 for Injector 1 and 0.172 for Injector 2, and at 12 kV they are 0.074 and 0.138. Figure S4b shows the all-region ratio $\mathcal{R}_{32}$ against I^*. At 12 kV, $\mathcal{R}_{32}$ is 0.48 (interval 0.39 to 0.66) for Injector 1 and 0.80 (interval 0.69 to 0.91) for Injector 2. The decrease with I^* is larger for Injector 1, and the two curves remain separated.

The net current per unit liquid flow rate,

$$\rho_{q,\mathrm{app}} = \frac{|I_{\mathrm{net}}|}{Q_l},$$

is an apparent charge per unit liquid volume, because the global current does not identify the charge carried by the droplets alone. It takes the values of 126 C m^{-3} for Injector 1 and 65 C m^{-3} for Injector 2 at 12 kV. Figure S4c shows $\mathcal{R}_{32}$ against $\rho_{q,\mathrm{app}}$ on a symmetric-logarithmic horizontal axis, which retains the zero-voltage reference at zero. Over the range where the two injectors overlap, up to about 65 C m^{-3}, the sampling intervals of the all-region values of the two injectors overlap. For example, at 64 and 65 C m^{-3} the values are 0.67 (interval 0.53 to 0.91) for Injector 1 and 0.80 (interval 0.69 to 0.91) for Injector 2. The highest point of Injector 1 (126 C m^{-3}) has no counterpart in Injector 2. Overlap of wide intervals does not demonstrate a common dependence, so this panel is an exploratory observation and not evidence of a collapse. A contribution of geometry or flow conditions cannot be excluded.

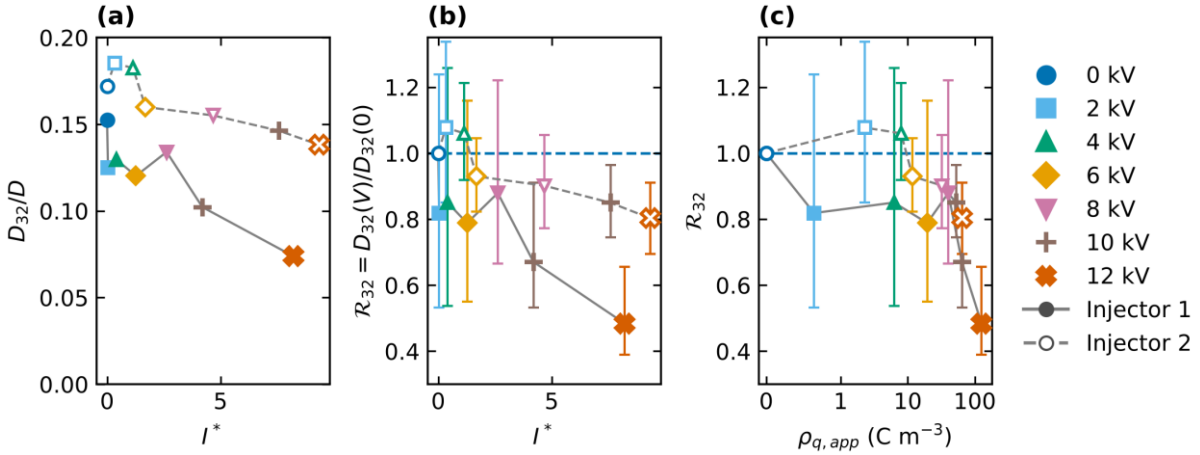

Figure S4. All-region response of the Sauter mean diameter for the two injectors, calculated from all accepted trajectories of each injector at each voltage, combining the five transverse regions ($0 \leq \xi \leq 0.5$). The values do not represent the whole spray. (a) Normalized Sauter mean diameter, D_{32}/D, against the normalized net current I^*. (b) Ratio $\mathcal{R}_{32} = D_{32}(V)/D_{32}(0)$ against I^*. (c) Ratio $\mathcal{R}_{32}$ against the apparent specific charge $\rho_{q,\mathrm{app}} = |I_{\mathrm{net}}|/Q_l$, with a symmetric logarithmic horizontal axis. Filled symbols and solid lines correspond to Injector 1 and open symbols and dashed lines to Injector 2. Symbols and colors indicate the applied voltage. Error bars in (b) and (c) are 95% sampling intervals obtained by resampling recordings and then trajectories (Sect. S5).

References

Gañán-Calvo, A. M.: On the general scaling theory for electrospraying, J. Fluid Mech., 507, 203–212, 2004.

Gañán-Calvo, A. M., Dávila, J., and Barrero, A.: Current and droplet size in the electrospraying of liquids. Scaling laws, J. Aerosol Sci., 28, 249–275, 1997.